RAPID COMMUNICATIONS

PHYSICAL REVIEW B VOLUME 52, NUMBER 2 1 JULY 1995-II

Indirect exchange coupling for orthogonal anisotropies

H. J. Elmers, G. Liu, H. Fritzsche, and U. Gradmann
Physikalisches Institut, Technische Universität Clausthal, D-38678 Clausthal-Zellerfeld, Germany
(Received 26 January 1995)

In magnetic trilayers W(110)/Fe/Cr/Fe/Cr, the in-plane anisotropies can be tailored in such a way that the easy axis of the first Fe film is along $[1\bar{1}0]$ and that of the second one along [001]. Magnetization loops of those samples with orthogonal anisotropies were observed by Kerr magnetometry. From fitting the loops, both bilinear and biquadratic coupling constants could be determined independently.

Indirect exchange coupling of ferromagnetic films through a nonmagnetic spacer layer has been an active field since its observation in Fe(100)/Cr(100)/Fe(100) trilayers[1] and the observation of the oscillatory dependence of its leading Heisenberg-like term on interlayer spacing.[2] Experimentally, antiferromagnetic coupling can easily be inferred from the magnetization loop or from giant magnetoresistance,[3] whereas the measurement of ferromagnetic coupling requires more sophisticated methods like Brillouin light scattering (Ref. 4) or ferromagnetic resonance.[5] The period of the oscillation between ferro- and antiferromagnetic "bilinear" coupling is well understood.[6,7] Even the amplitude can now be calculated correctly.[8] A general review of indirect coupling is given in Ref. 9.

In addition to the bilinear coupling, one observes in specific cases a so-called "biquadratic" coupling, which supports a 90° orientation of the magnetization in the coupled layers. Originally introduced in order to explain the magnetization reversal in Fe/Cr/Fe(100) trilayers,[10] it has been observed in Co(0001)/Cu(111)/Co(0001),[11] Fe/Al/Fe(100),[12,13] Fe/Au/Fe(100),[13] Fe/Ag/Fe(100),[14] γFe/Cu/Fe(100),[5] and FeCo/Mn/FeCo(100).[15] Biquadratic coupling coefficients are hard to determine and frequently cannot be separated from the bilinear coupling coefficients.[13] Available models of biquadratic coupling include a spin-flop-like mechanism resulting from interface roughness,[16,17] the role of "loose spins" in the spacer[18] and intrinsic mechanisms[19–22] of electronic origin. At present, none of the available models is able to quantitatively explain the experiments, the theoretical predictions typically being one or several orders too low in comparison with the experimental data.

In this paper, we present an experimental approach to indirect coupling. This method offers the possibility of independent and straightforward determination of both bilinear and biquadratic coupling from one single measurement. The method is based on a trilayer containing two uniaxial magnetic films with orthogonal easy axes. For comparison, nearly all previous experiments on indirect coupling have been done using samples in which both magnetic layers showed the same fourfold or sixfold in-plane symmetry, e.g., Fe(100) or Co(0001). All studies of biquadratic coupling used samples of this type. Coupling between uniaxial magnetic films has been investigated in two papers only. Grünberg *et. al*[4] investigated coupling in Fe/Cr/Fe(110) sandwiches, Fullerton *et. al*[23] in Fe/Cr(211) superlattices. However, contrary to our approach, the easy axes of the coupled films were parallel in those previous studies. To our knowledge, coupling in trilayers with orthogonal anisotropies has not been studied before.

In order to explain the method, we consider a trilayer consisting of two uniaxial ferromagnetic layers with orthogonal easy axes in the plane, coupled by a nonmagnetic spacer layer. An external field H is applied along the easy axis of layer (1) of thickness t_1, the *driver layer*. This axis by definition is the x axis of a Cartesian system. The easy axis of layer (2), of thickness t_2, the *sensor layer*, is the y axis. Let us consider the anisotropies in a quadratic approximation, the anisotropy energy per area of layer (i) being given by $f_{k,i}(\varphi_i)=k_i\cos^2\varphi_i$ ($i=1,2$; azimuth φ_i of the magnetization in layer i with respect to the x axis), with $k_1<0$ for the driver, $k_2>0$ for the sensor layer. Without coupling, the loop of the sample is the superposition of an easy axis loop of the driver with the hard axis loop of the sensor layer.

For the coupling energy per area, we write (following Ref. 9) $f_{12}(\varphi_1-\varphi_2)=-J_1\cos(\varphi_1-\varphi_2)-J_2\cos^2(\varphi_1-\varphi_2)$. The aim then is the determination of the bilinear and biquadratic coupling constants J_1 and J_2 from the equilibriums sections of the magnetization loop. They result from a minimization of the free enthalpy per area, $q(\varphi_1,\varphi_2)=f_{k,1}(\varphi_1)+f_{k,2}(\varphi_2)+f_{12}(\varphi_1-\varphi_2)-J_sH(t_1\cos\varphi_1+t_2\cos\varphi_2)$, where $J-s$ is the saturation magnetic polarization. The loop can be easily understood if the driver anisotropy is strong enough to obtain $\varphi_1=0$ for decreasing positive fields. This may be realized by weak coupling, $J_1\ll|k_1|$, $J_2\ll|k_1|$, or by a weak sensor anisotropy, $k_2\ll|k_1|$. In this *rigid driver model*, g depends on φ_2 only, for decreasing $H>0$. By introducing an exchange field $H_A=J_1/(J_st_2)$, an anisotropy field $H_{k,2}=2k_2/(J_st_2)$ and an effective anisotropy field $H_{k,\mathrm{eff}}=[2k_2-2J_2]/(J_st_2)$, g may be written as

$$g(\varphi_2)=(J_st_2)\{H_{k,\mathrm{eff}}\cos^2\varphi_2-(H+H_A)\cos\varphi_2\}. \quad (1)$$

Minimization of g then results in $\cos\varphi_2=(H+H_A)/H_{k,\mathrm{eff}}$. The effect of the coupling consists in a shift of the sensor loop by $(-H_A)$ and a change of its initial slope from $1/H_k$ to $1/H_{k,\mathrm{eff}}$. If $H_{k,2}$ is available from the loop of the bare sensor, both coupling constants can be determined easily as $J_1=(J_st_2)H_A$ and $J_2=(J_st_2/8)(H_{k,2}-H_{k,\mathrm{eff}})$.

In a more general case, we use a fourth-order approximation $f_{k,i}(\varphi_i)=k_i\cos^2\varphi_i+l_i\cos^4\varphi_i$ for the single-layer anisotropies and determine the sample loops by numerical minimization of g. Examples of calculated loops are shown

 © 1995 The American Physical Society

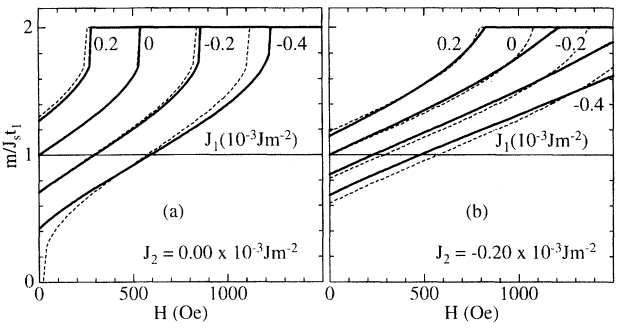

FIG. 1. Calculated magnetization loops for trilayer samples with orthogonal anisotropies and symmetric thickness $t_1=t_2=t=4$ nm of driver (1) and sensor (2) layer. Magnetic moment component m per area along the field direction [001] versus magnetic field H, in units of the driver saturation moment $J_s t_1$. The full line shows the result of numerical minimization of the free enthalpy g. Magnetization $J_s=2.17$ T of bulk Fe is used. Anisotropy parameters $k_1=+0.35\times10^{-3}$ J m^{-2}, $l_1=-0.09\times10^{-3}$ J m^{-2}, $k_2=-0.90\times10^{-3}$ J m^{-2} and $l_2=-0.15\times10^{-3}$ J m^{-2} representing the experimental samples of Fig. 3. Coupling constants J_1 as parameters. $J_2=0$ and $J_2=-0.20\times10^{-3}$ J m^{-2} in (a) and (b), respectively. Results of the rigid driver model for comparison by dotted lines.

in Fig. 1 by full lines. By restricting the presentation to positive decreasing fields, we avoid hysteresis problems in the driver loop. The single film anisotropy constants are taken from the experimental samples to be discussed below. The result of the rigid driver model ($|k_1|=\infty$) are given by dotted lines for comparison. The validity of the rigid driver model for weak coupling or weak sensor anisotropies is obvious. The shift of the loop by bilinear coupling, combined with a change of the initial slope by biquadratic coupling, is a common feature of the rigid driver model and the numerical evaluation. The jumplike transition to saturation is determined by the fourth-order component of the sensor anisotropy.

In realizing trilayer structures with orthogonal anisotropies, we took advantage of our recent study of anisotropies of Fe(110) interfaces.[24] In particular, we used the fact that the W(110)/Fe(110) interface strongly supports the in-plane [110] axis, whereas a Fe(110)/Cr(110) interface supports the bulk easy in-plane axis [001]. Accordingly, we used samples of type W(110)/Fe/Cr/Fe/Cr, as shown schematically in Fig. 2. The films were prepared in UHV by epitaxy on W(110), starting with a sensor Fe layer of constant thickness $t_2=D_2 d$ (typically abut 4 nm), consisting of D_2 atomic layers of interlayer spacing d. It was deposited in an optimized mode described previously,[25] starting at a substrate temperature $T_s=300$ K in order to avoid Stranski-Krastanov islanding, ending up with $T_s=600$ K in order to obtain atomically smooth Fe(110) surfaces with an average terrace width of 50 nm.[26] All further layers were prepared at 300 K. The sensor layer was covered by a Cr interlayer of wedgelike increasing thickness $t_{Cr}=D_{Cr}d$ (we neglect the minor difference in Fe and Cr lattice spacings), followed by the driver layer of constant thickness $t_1=D_1 d$ and a final Cr coverage. One end of the sample was kept free from the driver, in order to determine the sensor anisotropies from the bare sensor loop. All layers were structurally coherent with the basic Fe sensor layer, as tested by high angular resolution low-energy electron diffration (HRLEED).

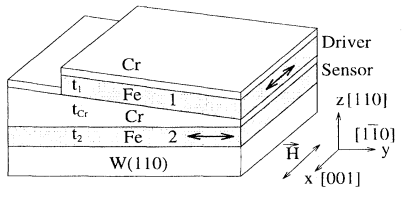

FIG. 2. Structure of the samples, schematic.

The in-plane anisotropies are proper superpositions of volume and surface anisotropies. For the driver, both of them support [001]. The driver magnetization therefore is strongly coupled to [001]. For the sensor, as a result of the strong anisotropies of the W(110)/Fe(110) interface, the easy axis is directed along $[1\bar{1}0]$ up to a thickness of about 6 nm, where it is rotated towards [001] as a result of the increasing volume anisotropies, supported by the Fe/Cr interface. Accordingly, the magnetization in our sensor layers of 4 or 5 nm thickness was weakly coupled to $[1\bar{1}0]$, as required. Numerical data of anisotropies are given in the caption of Fig. 3.

Magnetization loops were measured using the magneto-optical Kerr-effect. We used the longitudinal Kerr effect (oblique incidence of s-polarized light), probing the longitudinal magnetization component in the plane of incidence. The external field being in this plane too, we measured the usual magnetization loop $m(H)=m_1(H)+m_2(H)$, m_i being the moment component of layer (i) along the field axis. The Kerr rotation was compensated using a Faraday rotator and lock-in techniques as described in Ref. 27. Our primary signal is the dc current I of the rotator. The evaluation in terms of m was based on two observations coming from auxiliary experiments: (i) In our samples, I is proportional to m, independently on the distribution between m_1 and m_2, up to the maximum total Fe thickness of 8 nm. (ii) I decreases linearly with t_{Cr}, again independently on the relative contributions of m_1 and m_2 to m. This second observation is compatible with a picture of the Kerr effect as resulting from a reflection of the light from the W substrate, with Faraday rotations of both the incident and the reflected light. Accordingly, we used as a basis for our evaluation a relation $I=C(m_1+m_2)(1-t_{Cr}/\xi)$ between I and the sample moment (m_1+m_2), with an empirical value of $\xi=14$ nm, and an appropriate constant C. The validity of this evaluation was checked using samples for which the sensor layer could be saturated using the available field, and where coupling could be neglected, e.g., the sample with $D_{Cr}=29.7$ in Fig. 3(a). Neglecting all coupling in this sample, in view of the large interlayer thickness, we assume $m_2(0)=0$ and $m(0)/m_1=1$, which we use to calibrate the vertical axis. We then expect a saturation value $m_{sat}/m_1=39.9/20.2=1.975$, in excellent agreement with the experimental result $m_{sat}/m_1=1.97$.

A systematic analysis of the coupling phenomenon as a function of D_{Cr} was performed using samples of roughly symmetric Fe thickness, $D_1\approx D_2\approx 20$ monolayer (ML), and a wedgelike increasing number D_{Cr}. Examples of magnetization loops are shown in Figs. 3(a)–3(f). For D_{Cr}

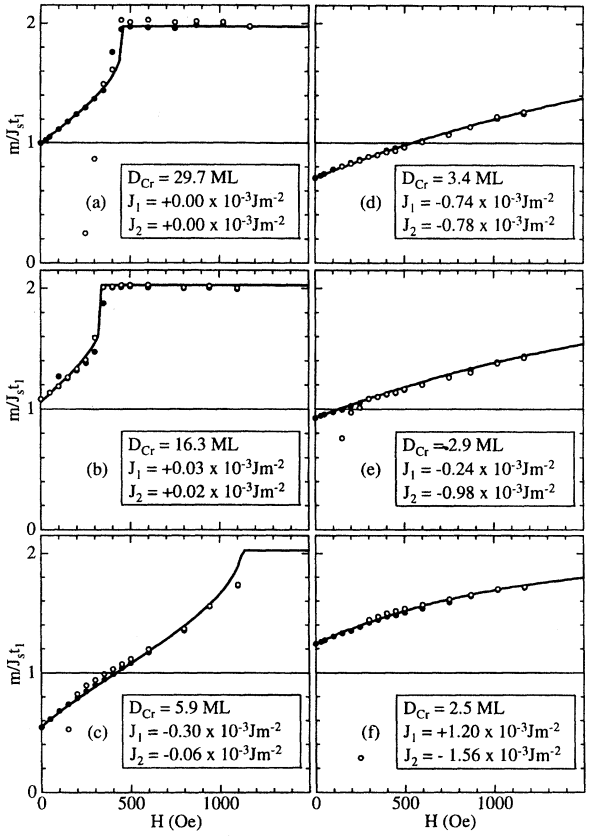

FIG. 3. Experimental magnetization loops $m/(J_s t_1)$ versus H for samples W(110)/D_1Fe/D_{Cr} Cr/D_2Fe/5 Cr with symmetric thickness $D_1 \approx D_2 \approx 20$. More precisely, $\{D_1/D_{Cr}/D_2\}$ are given by (a) {20.2/29.7/19.7}, (b) {19.0/16.3/19.5}, (c) {19.0/5.9/19.5}, (d) {19.7/3.4/21.3}, (e) {19.7/2.9/21.3}, and (f) {19.7/2.5/21.3}, respectively. Closed circles for decreasing, open circles for increasing fields. Full lines are fitting curves from minimization of g, resulting in the coupling parameters as included.

$=29.7$ [Fig. 3(a)], where the coupling can be neglected, the undeformed sensor loop is superimposed on the constant driver moment $m_1 = J_s t_1$. For $D_{Cr} = 16.3$ [Fig. 3(b)], the shift of the loop indicates a weak ferromagnetic coupling, and the increase of the initial slope indicates a weakly positive J_2. For the other values of D_{Cr}, dramatic changes in the sensor loop are observed, both for the initial slope, and for the loop shift. In order to determine the coupling parameters from the loops, one needs the single-layer anisotropies from independent measurements. The sensor anisotropies could be determined from the hard axis loop of the bare sensor layer; see Fig. 2. The driver anisotropies were determined from our previous work.[24] Using these anisotropies, the loop fitting resulted in the coupling parameters which are included in Fig. 3.

As a result of an analysis such as that in Fig. 3, we show in Fig. 4(a) the bilinear coupling parameter J_1 and in Fig. 4(b) the biquadratic parameter J_2, both versus D_{Cr}, from two samples, both with $D_1 \approx D_2 \approx 20$ ML. Full evaluation by numerical simulation (full symbols) was performed for a selected group of loops only. Results obtained using the rigid

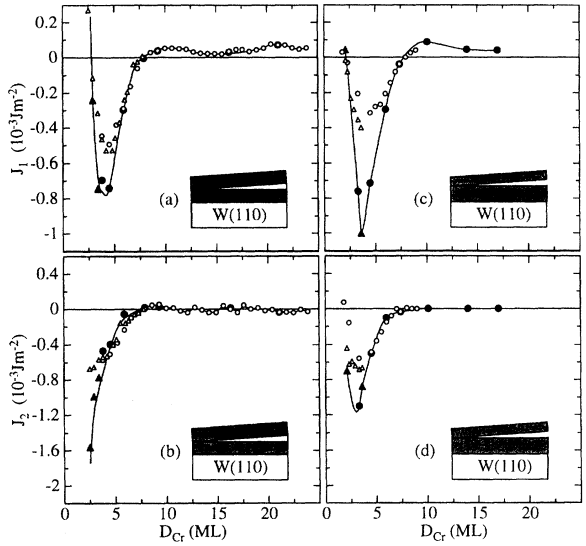

FIG. 4. Coupling parameters J_1 (a) and J_2 (b) versus D_{Cr} for sandwiches with symmetric thickness of Fe layers, $D_1 \approx D_2 \approx 20$. Circles and triangles from different samples. Full symbols from numerical simulation, open symbols from the rigid driver model. (c) and (d) as (a) and (b), respectively, but for $D_1 \approx 13$, $D_2 \approx 25$.

driver model (open symbols) are shown for comparison. As expected, the differences are small for the case of weak coupling. The oscillation of J_1 above $D_{Cr} = 10$ could therefore be obtained using the rigid driver model. The measurements for the samples with symmetric Fe thickness were supplemented by samples with asymmetric Fe thickness, roughly $D_1 = 25$, $D_2 = 13$. The resulting coupling parameters J_1 and J_2 are shown in Figs. 4(c) and 4(d), respectively. As a common gross feature of both series, we observe strong antiferromagnetic extremum with $J_1 = -0.8(-1.0) \times 10^{-3}$ J m^{-2} (values for the second series, Figs. 4(c) and 4(d), in brackets) at $D_{Cr} = 4.0(3.6)$ ML, that means $t_{Cr} = 0.80(0.72)$ nm, between zeros at $D_{Cr} = 0.29(0.22)$ and 0.79(0.79) ML, or $t_{Cr} = 0.58(0.44)$ and 1.58(1.58) nm. This is in excellent agreement with previous work of Grünberg *et al.*,[4] who observed an antiferromagnetic minimum of $J_1 = -0.7 \times 10^{-3}$ J m^{-2} at $t_{Cr} = 0.7$ nm between zeros at 0.45 and 1.45 nm. Both series show a ferromagnetic maximum at $D_{Cr} = 11(10)$ ML. A second maximum at 22 ML is found only in the first series, a common minimum in both series at $D_{Cr} = 15(16)$ ML. As a whole, we observe a long-period oscillation of J_1 with a period of $\Delta D_{Cr} = 11$ ML or $\Delta t_{Cr} = 2.2$ nm. This is similar but definitely different from the results of Fullerton *et al.*[23] for the case of Fe/Cr(211) and Fe/Cr(100) superlattices, for which they reported a common period of $\Delta D_{Cr} = 9$ ML or $\Delta t_{Cr} = 1.8$ nm. In both series we observe a strong biquadratic coupling for $D_{Cr} < 7$ ML. Details are different: a clear extremum of J_2 at about $D_{Cr} = 3$ ML for the samples with asymmetric thickness cannot be found in the symmetric samples. The magnitude of the biquadratic coupling is again surprisingly large. WE can only speculate on the origin of this strong coupling. The most probable interpretation, in our opinion, is a modified version of Slonczewskis first spin-flip model.[16] A HRLEED analysis of a Cr

layer of about 3 ML, near the extremum of J_2 in Fig. 4(d), shows a considerable interface width of about 5 ML. If this would include long range fluctuations of the film thickness, similar as observed for the autoepitaxy of Fe on Fe(110),[28,26] an interlayer of 3 ML Cr could consist of rather extended areas of opposite sign of the coupling, for $D_{Cr} \geqslant 3$ ML and $D_{Cr} \leqslant 2$ ML, respectively. Because the magnitude of J_2, in Slonczewskis model, increases with the width of the homogeneously coupling areas, a comparatively large width which is not unreasonable in our model could roughly explain the large value of J_2. The clear dependence on the thickness of the driver layer supports this idea. However, further experiments including detailed analysis of the film structure are obviously needed for a full understanding of the biquadratic coupling.

In conclusion, we have shown that magnetization loops of indirectly coupling trilayers with orthogonal anisotropies of the ferromagnetic layers provide a useful method for measuring both bilinear and biquadratic indirect exchange coupling parameters. Coherent epitaxial samples W(110)/Fe/Cr/Fe/Cr can be tailored to provide those orthogonal anisotropies in the film plane. The evaluation of their magnetization loops results for the bilinear coupling in a strong antiferromagnetic minimum of $J_1 = -(0.9 \pm 0.1) \times 10^{-3}$ J m^{-2} near $D_{Cr} = 4$ ML, followed by a weak oscillation with a period of about 11 ML Cr. For the biquadratic coupling parameter, strong values down to $J_2 = -1.6 \times 10^{-3}$ J m^{-2} were detected. The method allows one to measure even positive values of J_2, which actually are observed in some of our samples.

This work was supported by the Deutsche Forschungsgemeinschaft.

[1] P. Grünberg *et al.*, Phys. Rev. Lett. **57**, 2442 (1986).
[2] S. S. P. Parkin *et al.*, Phys. Rev. Lett. **64**, 2304 (1990).
[3] F. Petroff *et al.*, Phys. Rev. B **44**, 5355 (1991).
[4] P. Grünberg *et al.*, J. Magn. Magn. Mater. **93**, 58 (1991).
[5] B. Heinrich *et al.*, Phys. Rev. B **47**, 5077 (1993).
[6] D. M. Edwards *et al.*, Phys. Rev. Lett. **67**, 493 (1991).
[7] P. Bruno and C. Chappert, Phys. Rev. B **46**, 261 (1992).
[8] M. Villeret *et al.*, J. Magn. Magn. Mater. (to be published).
[9] A. Fert *et al.*, J. Magn. Magn. Mater. **140-144**, 1 (1995).
[10] M. Rührig *et al.*, Phys. Status Solidi A **125**, 635 (1991).
[11] B. Heinrich *et al.*, Phys. Rev. B **44**, 9348 (1991).
[12] C. J. Gutierrez *et al.*, J. Magn. Magn. Mater. **116**, L305 (1992).
[13] A. Fuss *et al.*, J. Magn. Magn. Mater. **103**, L221 (1992).
[14] J. Unguris, R. J. Celotta, and D. T. Pierce, J. Magn. Magn. Mater. **127**, 205 (1993).
[15] J. J. Krebs *et al.*, J. Magn. Magn. Mater. (to be published).
[16] J. C. Slonczewski, Phys. Rev. Lett. **67**, 3172 (1991).
[17] S. Demokritov *et al.*, Phys. Rev. B **49**, 720 (1994).
[18] J. C. Slonczewski, J. Appl. Phys. **73**, 5957 (1993).
[19] R. P. Erickson, K. B. Hathaway, and J. R. Cullen, Phys. Rev. B **47**, 2626 (1993).
[20] D. M. Edwards, J. M. Ward, and J. Mathon, J. Magn. Magn. Mater. **126**, 380 (1993).
[21] J. d.'A. e Castro, M. S. Ferreira, and R. B. Muniz, Phys. Rev. B **49**, 16 062 (1994).
[22] J. Inoue, J. Magn. Magn. Mater. **136**, 233 (1994).
[23] E. E. Fullerton *et al.*, Phys. Rev. B **48**, 15 755 (1993).
[24] H. Fritzsche, H. J. Elmers, and U. Gradmann, J. Magn. Magn. Mater. **135**, 343 (1994).
[25] H. J. Elmers and U. Gradmann, Appl. Phys. A **51**, 25 (1990).
[26] M. Albrecht, H. Fritzsche, and U. Gradmann, Surf. Sci. **294**, 1 (1993).
[27] H. Hornauer, T. M. Atmono, and K. Röll, J. Magn. Magn. Mater. **83**, 551 (1990).
[28] H. Fritzsche and U. Gradmann, in *Common Themes and Mechanisms of Epitaxial Growth*, edited by P. Fuoss *et al.*, MRS Symposia Proceedings No. 312 (Materials Research Society, Pittsburgh, 1993), p. 321.

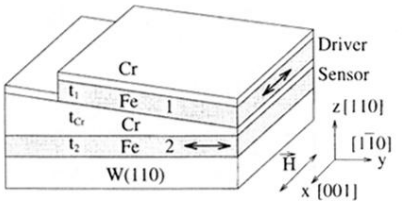

FIG. 2. Structure of the samples, schematic.